JETIR.ORG ISSN: 2349-5162 | ESTD Year : 2014 | Monthly Issue
JOURNAL OF EMERGING TECHNOLOGIES AND INNOVATIVE RESEARCH (JETIR)
An International Scholarly Open Access, Peer-reviewed, Refereed Journal

THE PETROGENESIS OF MAFIC ENCLAVES AND LADAKH GRANITOIDS IN THE SOUTHERN MARGIN OF LADAKH BATHOLITH: EVIDENCE OF MAGMA MIXING AND CHEMICAL EQUILIBRIUM

C. Perumalsamy[1*]

[1]Wadia Institute of Himalayan Geology, 33, GMS Road, Dehradun – 248001, India.

Abstract: *The subduction of Neotethyan oceanic slab-derived fluids/melts generates a metasomatized lithospheric mantle beneath the Eurasian margin. The mafic enclaves formed by the subduction-modified mantle source derived mafic magmas with intense fractional crystallization and late-stage assimilation of felsic magmas of Neotethyan amphibolite lower crustal melting. The I-type Ladakh granitoids were generated by mantle-derived mafic mixing with felsic magmas of the heterogeneous melting of the heterogeneous source rocks of low to high K Neotethyan amphibolite lower crust, KLA tonalitic lower crust and northern Indian margin metasediments in the active margin of the Eurasian plate. The formation of mafic enclaves and Ladakh granitoids related to the subducted Neotethyan slab roll-back induced asthenospheric mantle upwelling and the initial contact between Indian and Eurasian plates.*

Keywords: *Mafic enclaves, granitoids, Metasomatism, Geochemistry, Magma mixing, Slab roll-back.*

I. Introduction

The common occurrence of mafic enclave (ME) in calc-alkaline granitoids provides information about the interaction between the continental crust and mantle and geodynamic setting [8,7, 30, 72]. The direct mantle partial-melting, oceanic slab, metasomatized mantle, and lower and upper continental crusts are the main source for a wide range of granitoids generation within the continental crust [6]. The mafic enclaves together with its host felsic rocks are grouped into, 1) xenolith or partially digested fragments of country rocks on the margin of the granitic pluton, ii) the segregation or separation of source material (restite) left after the partial melting event, iii) early crystallized ferromagnesian mafic phases chilled (cognate or autolith) on the margin of the felsic pluton, iv) the mafic magmas entrained into the felsic magmas, mixing and mingling with its felsic host magmas (hybrid magmas), and v) the intrusion of mafic dyke at any stage of felsic magma evolution [1,28]. I-type calc-alkaline granitoids are metaluminous to slightly persubduction-modifie1.1), with mafic to felsic regular inter-elemental variations [11,12]. High-K calc-alkaline I-type granitoids are associated with subduction zone processes where melts are generated in mantle wedges

and enriched through interaction with fluids from down-going, dehydrating slabs [45]. The geochemical and isotopic variations between mafic microgranular enclave or mafic rocks and its host calc-alakline granitoids as evidence of mixture of crust and mantle components in the source of batholiths [56,58].

Collisional orogens involve three stages: transitional subduction of oeanic lithosphere into the continental collision and continental subduction. The studies on the Transhimalayan magmatic rocks in the southern margin of the Eurasian plate reveals the prolonged subduction of Neotethyan oceanic lithosphere, subsequent contamination by Indian crustal contamination or crustal sediments assimilation [24]. Himalayan orogenic belts resulted from the consumption of the Neotethyan ocean, followed by India and Eurasia collision and convergence since early Palaeocene to early Eocene (~65 Ma to ~45 Ma). The ~2500 km long, calc-alkaline Transhimalayan magmatic arc (TMA) genesis is related to the subduction of the Neotethyan oceanic lithosphere along the southern margin of the Eurasia plate, subsequent the subduction of Indian lithospheric mantle beneath the Eurasian margin [57,1,26,54,58,68]. TMA is classified into the western Kohistan-Ladakh intra-oceanic magmatic arc (KLA), and eastern Gangdese continental-type plutonic complex. It has (TMA) mainly composed of biotite- and hornblende-bearing granodiorite with less abundance of primitive olivine norite, gabbro, evolved biotite granite, tonalite, and late-stage leucogranitic dikes [62]. However, the petrogenesis of the mafic enclaves and their host Ladakh granitoids in the southern margin of Ladakh batholiths related to the subduction of Neotethyan oceanic lithosphere to the initial contact between Indian and Eurasian plates remains controversial and still poorly understood. This study includes detailed petrography, whole rocks major, tracer geochemistry for the mafic enclaves and its host Ladakh granitoids to constraint the formation and evolution of the mafic enclave and its host Ladakh granitoid in the southern margin of the Ladakh batholith.

II. Geological setting of the Indus Suture zone

2.1. Indus Suture zone (ISZ)

This zone marks the collisional boundary between the northern Indian continental margin (Zanskar Backthrust) and the southern edge of the Eurasian plate (Ladakh Batholiths) from NW Pakistan, through Ladakh and southern Tibet to the eastern Hgranitoidimalayan Syntaxis, where Indian and Eurasian crustal rocks exposed. This zone comprises the different tectono-stratigraphic units of the Lamayuru Complex, ophiolitic melange, Dras arc complex, Indus Formation and Ladakh batholith from south to north. Ladakh Indus Suture consists of mainly Nidar, shergol and spongtang ophiolitic melange of Cretaceous to Tertiary age [37,3,64,65].

2.2 Indian plate

The hanging wall of the Zanskar Shear zone separates the Indus Suture zone from the northern passive continental margin of the Indian plate. This Indian plate in the Indus Suture zone consists of three laterally deposited supra crustal rocks, Paleo to Neo Proterozoic Lesser Himalayan Sequence (LHS), Neo-Proterozoic to Ordovician Greater and Tethyan Himalayan Sequence (GHS, LHS) separated by MCT and STD [60,62]. The northern Gondwana margin of the Indian plate consists of Precambrian Greater Himalayan orthogneisses and supra-crustal metasedimentary rocks of metapelites (Mg-rich metapelite, Fe-metapelite and intermediate metapelite) and metagreywackes (GHCS) intruded by 500 Ma granite [19,20,13,2,14,48,64].

2.3 Asian plate

India's northward drift, the early Cretaceous to early Eocene subduction of Neotethyan lithosphere mantle beneath the active Andean-type southern margin of Asia resulting in the intrusion of 2500 km long calc-alkaline, I-type Transhimalaya arc magmatism from the western Kohistan batholith in Pakistan, central NW Ladakh batholith in India, and eastern Gangdese batholith in Tibet and the cessation of calc-alkaline arc magmatism after the onset of collision between India and Eurasian plates [1,9,22,58,67,68,70]. Kohistan–Ladakh intra-oceanic volcanic Arc (KLA) is located between the Shyok Suture Zone (SSZ) and Indus-Tsangpo Suture Zone (ITSZ), as a result of the north-dipping subduction of the Neo-Tethyan oceanic crust beneath the KLA. Kohistan–Ladakh batholith shows two intrusive episodes of magmatisms, (1) the 103–83 Ma mafic-ultramafic rocks and arc-related volcanic rocks and (2) the 67–50 Ma diorite-granodiorite-granite (Ravikant et al., 2009). Calc-alkaline granitoids forms the bulk of the Ladakh batholith of the NW Indian Transhimalaya, while the western Kohistan batholith forms the Kohistan–Ladakh magmatic arc. Among Ladakh batholiths (LG) is bounded by the Indus Suture zone in the south, the Shyok Suture zone in the north, the Karakoram fault in the east and the Nanga Parbat-Haramosh massif [21,28,29,46,49]. The felsic magmatism in the north of the Indus Suture zone is known as Ladakh granitoid or granite (LG), whereas the felsic magmatism associated with mafic magmatic enclaves constitutes the Ladakh Batholith (LB) [28]. It has 600 km long, 30-80 km wide, and approximately 3 km thick from NW Astor, Deosai, and Skardu to SE Demchuk, Leh, Upshi, and Lyoma [28,59,65]. It consists of a complex sequence of gabbroic to granite plutons with mafic micro-granular enclaves consist of biotite-amphibole bearing granodiorite and granite, less tonalite-diorite, qz-monzodiorite-granodiorite, bt-amp bearing granite, pink porphyritic granite, leucogranite along pegmatitic dykes [21,28,46,4751,57,67]. The estimated composition of 10-

20 vol.% of mafic rocks, 20-30 vol.% of intermediate rocks and 50 vol.% granodiorites in Ladakh batholiths suggested that the multistage mixing and mingling of coeval mafic and felsic magmas for the formation of the Ladakh batholith [57,59]. The shallow crustal magma chamber derived two end member magma mixing and fractional crystallization processes generate hybrid mafic enclave (diorite, monzodiorite, quartz-diorite, tonalite and granodiorite) and their evolved host Ladakh granite. The Ladakh batholith in north-western India comprises dominantly an 'calc-alkaline I-type' suite of igneous bodies in subduction zone environment [62]. The magmatic ages for the Ladakh Batholith fall cluster between c. 75 and 45 Ma and its initial $^{87}Sr/^{86}Sr$ and $^{143}Nd/^{144}Nd$ ratios yield chondritic values [5,9,22,46,57,58,59,62,67,70].

III. Sample collection and analytical methods

3.1 Major oxide measurement

The mafic enclaves (no: 05) and granitoids (no: 11) were collected in the southern margin of Ladakh batholiths, Indus Suture zone. The details sample locations are marked on the geological map (Fig. 1), and their coordination is given in Table 1. Fresh whole rock sample chips were made finely powdered (-200 mesh size) using a tungsten carbide vibrating cup mill (Insmart systems). Six grams of each sample were taken and made into a pressed powder pellet (PPP) at a pressure of ~ 200 MPa for 2 min by mixing with five drops of saturated aqueous polyvinyl alcohol solution [52]. The major oxides were measured using a wavelength dispersive X-ray fluorescence (WD-XRF), S-8 Tiger series Bruker at Central Laboratory, WIHG [52]. All major oxides were calibrated and validated using USGS reference materials (BCR-I, BCR-II, and BVRO). The precision and accuracy obtained for all major oxides were <5 %. The ignition on loss (LOI) was determined for all the samples before major oxide measurement. For that, 5 g of a powdered sample was taken in a silica crucible and kept in a furnace at 900°C for two hours. The detailed procedure was given elsewhere [53]. The results of major oxides and LOI are given in Table 2.

3.2 Trace elements analysis

Trace elemental analysis, including REE and Sr and Nd isotope ratio measurement, was carried out at the National Facility for Isotope Geosciences, Department of Earth Sciences, Pondicherry University, India. The precisely weighted 200 mg of -200 mesh size powdered samples were taken in a 7 ml Savilex® vial for decomposition. The acid mixture of HF: HNO_3: HCl (7:3:1 ratio) was added to the sample and heated on a hot plate at 130°C for 24 h. Samples were repeatedly dissolved and evaporated with HNO_3 and HF (3:1 ratio) to obtain a clear solution without fluoride crystals. The digestion procedure followed in this study was explained in detail elsewhere [25]. The dried sample was dissolved with 30 ml of 2 % HNO_3 for further analysis. The digested sample was split into two parts likely, 20 % of sample and 80 % of sample aliquot respectively. The 20% of the sample aliquot was used for trace element analysis. The trace elements, including rare earth elements, were measured using Inductively Coupled Plasma Mass Spectrometry (ICP-MS) (Thermo scientific X-series II) at the Department of Earth Sciences, Pondicherry University, Pondicherry. USGS reference materials were used to calibrate the instrument. The BHVO-2 and BCR-2 were used for the validation, and the precision and accuracy of analysis were less than 5% for most of the elements and less than 10% for all elements. The measured tracer element results are provided in Table 2.

3.3 EPMA plagioclase major elemental studies

The chemical composition of plagioclase was determined by a CAMECA SX-5 electron probe micro-analyzer (EPMA) with wavelength-dispersive spectrometry at EPMA Laboratory, Banaras Hindu University, Varanasi. The operating conditions were set an as accelerating voltage of 15 kV was maintained with a beam current of 12 nA and a beam diameter of 1 µm during the plagioclase major elemental analysis in the carbon-coated polished thin section of selective mafic enclaves and Ladakh granitoids. The crystal and elements PET-K, Ca, Ti, TAP-Si, Al, Mg, Na, P, and LIF- Fe, Cr, Mn, Zn, and Ni were set and analyzed. The precision for all major oxides is better than 1%.

IV. Analytical results

4.1 Field and petrographic observation

The mafic enclaves exhibit fine to medium grained spherical, globular, tabular to elongated shapes with sharp contact and less diffusive contact with the medium to coarse grained host granitoids (Fig. 2a-b).

The mafic enclaves dominantly fine to medium grained, porphyritic to interstitial texture, consisting of phenocryst of plagioclase, amphibole and biotite together with minor amount of K-feldspar, quartz, apatite, magnetite, ilmenite. The microtexture of mafic enclave shows the contact relationship between mafic enclave and host granite (Fig. 3a), the aggregated and interstitial growth of amphibole, biotite within plagioclase (Fig. 3b), a large phenocryst of amphibole and acicular apatite and amphibole (Fig. 3c) and resorbed plagioclase core undergone sericitic alteration (Fig. 3d).

Ladakh granitoid comprises mainly a large phenocrystal of plagioclase, K-feldspar, quartz, amphibole with accessory zircon, apatite and altered chlorite, epidote, magnetite. It shows generally perthite, graphic and myrkitic textures with a large quartz, k-feldspar phenocrystals intergrowth within a large phenocryst of plagioclases (Fig. 3e-h).

4.2 Whole-rock geochemistry

The whole rock geochemical compositions of mafic enclaves are given in Table. 2. The measured loss on ignition fall range from 1.34 wt.% to 4.08 wt.%. They have moderate SiO_2 (51.8-58.0), high Na_2O (2.90-3.83), K_2O (1.72-3.08), MnO (0.11-0.19), MgO (4.42-7.89), CaO (3.72-7.79), Fe_2O_3 (5.91-9.48), P_2O_5 (0.26-0.48), TiO_2 (0.93 & 1.26) with moderate to high $Mg^{\#}$ values fall range from 57-70. The mafic enclaves are monzodiorite, gabbrodiorite, monzonite in composition and I-type, metaluminous in nature with their alumina saturation index (A/CNK <1) (Fig. 4a, b). They are entirely high K calc-alkaline series on the K2O vs. SiO2 diagram and are magnesian nature based on FeO*/(FeO*+MgO) (Fig. 4c, d).

The major and tracer element data for Ladakh granitoids are given in Table 2. They show medium to high SiO_2 of 61.3-74.6 wt. %, Al_2O_3 of 14.6-16.9 wt. %, Na_2O of 3.74-5.60 wt. %, K_2O of 1.90-5.39 wt. %, with a low CaO of 0.98-4.38 wt. %, Fe_2O_3 of 0.52-5.00 wt. % and MgO of 0.12-2.90 wt. %, MnO of 0.01-0.13 wt. %, TiO_2 of 0.06-0.62 wt. %, P_2O_5 of 0.01-0.23 wt. %. The relatively low to moderate $Mg^{\#}$ values (27-56) for Ladakh granitoid than the mafic enclave. In the SiO_2 vs. (Na_2O+K_2O) diagram, the Ladakh granitoids are monzonite, Qz-monzonite and granite in composition (Fig. 4a) and I-type weak peraluminous nature with their ACK values of 1.0-1.1. They are belonging to high K calc-alkaline to shoshinitic affinity on SiO_2 vs. K_2O diagram (Fig. 4b) and magnesian in composition of calc-alkaline Ladakh granitoid with their FeO*/ (FeO*+MgO) values of 0.61-0.84 (Fig. 4c, d).

Chondrite-normalised rare earth element (REE) patterns for the mafic enclaves and host Ladakh granitoids show similar REEs patterns with the enrichment in LREEs, variable low HREE contents with the pronounced negative and positive Eu anomalies (δEu = 0.33–1.29 & δEu = 0.36–4.73). The mafic enclaves display mid to highly fractionated REE patterns (La/Yb_N = 6.52-20.7), while the host Ladakh granitoids exhibit low to highly fractionated REE patterns (La/Yb_N = 4.78-53.8). The mafic enclave and host granitoids have similar total REE concentration with the low to high total REE contents in Ladakh granitoids (ΣREE = 34.4-458.0) and moderate to high total REE contents in mafic enclaves (∑ = 101.7-298.9) (Fig. 5a).

On the primitive mantle-normalized trace element diagram, the Ladakh granitoids and mafic enclaves have similar tracer elemental patterns with the enrichment of large ion lithosphile elements in Rb, U (LILE) with sharp positive Pb spike, negative anomalies in Ba, Th, Nb, Ta, Zr, Hf anomalies and strong depletion in K, P, Ti. The Ladakh granitoids exhibits high level of LILEs, while the mafic enclave displays high level of HREE (Fig. 5b).

4.3 Plagioclase chemistry

The plagioclase chemical composition from the representative mafic enclave and host Ladakh granitoids are listed in Table. 3. The normal or simple plagioclase compositional zoning is observed in both mafic enclaves as well as in Ladakh granitoids (Fig. 6). The homogeneous, andesine composition from the core to rim of plagioclase phenocrysts in mafic enclave (ME-35) ($(An_{(0.34-0.36)}-Ab_{(0.62-0.65)})$; $(An_{(0.32-0.35)}-Ab_{(0.64-0.66)})$, while another mafic enclave (ME-45) exhibits core to rim of plagioclases have andesine to oligoclase composition ($(An_{(0.21-0.30)}-Ab_{(0.69-0.77)})$; $(An_{(0.22-0.31)}-Ab_{(0.68-0.77)})$. The core and rims of alkali feldspar in Ladakh granitoids falling orthoclase field ($An_{(0.00-0.00)}-Ab_{(0.00-0.07)}-Or_{(0.93-1.00)}$); ($An_{(0.00-0.00)}-Ab_{(0.02-0.06)}-Or_{(0.94-0.98)}$), while the core to rim of plagioclases are evolved Na-rich oligoclase composition ($An_{(0.06-0.21)}-Ab_{(0.78-0.88)}-Or_{(0.00-0.08)}$; ($An_{(0.18-0.19)}-Ab_{(0.81-0.82)}-Or_{(0.00-0.01)}$.

V. Discussion

5.1 Petrogenesis of mafic microgranular enclaves

The mafic enclaves are gabbro diorite, monzo gabbro, monzonite in composition, I-type, metaluminous, derived from high K calc-alkaline magma series (Fig. 4); [27,67]. The mafic enclaves are common in granitoids with the magmatic flow texture of plagioclase, amphibole and biotite, megacryst of amphibole, acicular apatite and megacryst of plagioclase with resorbed core suggesting that hot mafic magmas injected into cooler felsic mamas, subsequent a magma mixing and mingling involved in their petrogenesis (Fig. 2; Fig. 3); [28,29,36]. The mafic enclaves were derived from the metasomatized Neotethyan lithospheric mantle, which was earlier metasomatized by slab-derived fluids/melts (Fig. 7). The mafic enclaves are characterized by continental arc-type magmas with the enrichment of LILE (Rb, U) with sharp positive Pb spike, together with high LREE and depletion in HREEs and strong depletion in Nb, Ta, Zr, Hf, P, Ti, K, which is similar to metasomatized lithospheric mantle source with assimilation of crustal materials (Fig. 5); (Yang et al. 2007). The subduction slab-derived hydrous flux imparts the LILE-LREE enriched character to the overlying metasomatism of lithospheric mantle wedge in a continental margin arc setting [44]. The enrichment of LREE and strong depletion in HREE with flat HREE patterns indicates the presence of amphibole in the source region (Wang et al. 2020). The mafic enclaves have high K_2O (1.72-3.08) and potassic nature (K_2O/Na_2O = 0.50-1.03) suggesting that potassic phases such as amphibole, and phlogopite are in their mantle [23]. The variable K_2O contents and negative correlation with SiO_2 suggest that the successive removal of the potassic phase from the source region during the heterogeneous partial melting of transitional spinel-garnet-facies Iherzolite field (high La/Yb_N (6.46-47.9);

low Dy/Yb = 2.02-2.87), [15,34]. The mafic enclaves are phlogopite bearing peridotite melting than amphibole bearing mantle source regions by their high Ba/Rb (1.93-175) and Rb/Sr ratios (0.05-0.55), [55]. The upwelling mantle-derived mafic magmas melt mixing with felsic magmas of high K mafic rocks of Neotehthyan amphibolite lower crust melting derived, subsequent generation of mafic enclaves (Fig. 8), [35]. The Nb/Th and Zr/Nb ratios can use to identify the source of magmatic rocks [67]. The low Nb/Th (1.22-6.02) and Zr/Nb (0.19-1.70) ratios for mafic enclaves inferred that hydrous mantle derived mafic magmas with assimilation and magma mixing of granitic melts of crustal derived.
we suggest that the mafic enclaves were generated by partial melting of hydrous lithospheric mantle source, which was earlier modified by the subducted slab derived fluids/ melts, with subsequent intensive fractional crystallization of hydrous phases and late-stage assimilation and magma mixing of granitic hosts of the subducted Neotethyan oceanic amphibolite lower crustal melting.

5.2 Petrogenesis of Ladakh granitoids

The Ladakh granitoids are I-type, magnesian (weak peraluminous) derived from the medium to high K calc-alkaline magma series (Fig. 4).
The mafic enclave in granitoids with fine-medium grained plagioclase, K-feldspar, quartz megacrysts and the growth of apatite within plagioclase, perthitic, graphic textures in Ladakh granitoids represent the magma mixing processes (Fig. 2; Fig. 3), [36]. They are quartz-monzonite and granite in composition, intermediate to felsic composition (SiO_2= 61.3-74.6 wt.%) with mineral assembleage of plagioclase, K-feldspar, quartz phenocrystal in the fine grained plagioclase, K-feldspar, quartz and amphibole matrix (Fig. 3e-h); [29]. They are medium to high K calc-alkaline, metaluminous to slightly peraluminous (A/CNK < 1.1) signatures, and the abundance of hornblende and biotite represent the typical of I-type granitoids derived lithospheric mantle [67,74]. The mixture of mantle and crustal derived signature of Ladakh granitoids with high SiO_2 (61.3-74.6), MgO (0.12-6.95), Fe_2O_3 (0.52-7.85); TiO_2 (0.06-1.01), moderate to high Na_2O+K_2O (6.16-9.29); K_2O/Na_2O (0.34-1.44) (Yang et al. 2007). The negative correlation between P_2O_5 and SiO_2 and positive correlation Y, Th with increasing Rb inferred that the Ladakh granitoids belong to I-type granitoids (Fig. 9), [18]. The I-type granitoids produced by the mixing process, have similar REEs and tracer elemental patterns between the mafic enclaves and Ladakh granitoids by their chemical equilibrium during the mixing and mingling process (Fig. 5); [72]. The adakitic signature of variable REEs with the enrichment of LREEs than HREEs and negative to positive Eu anomalies reflect residual amphibole-garnet without plagioclase in the source rocks [23]. The high abundances of LILEs and LREEs, pronounced positive Pb and HFSE depletion with negative Ta-Nb-Zr-Hr-Ti-P-K anomalies indicate subducted oceanic slab modified lithospheric mantle derived magma mixing felsic magmas of continental crust derived [55]. Based on source discrimination diagram, the Ladakh granitoids straddle between on low to high K mafic rocks field, felsic rocks (tonalite) with less metasediments field. These observations indicate that the Ladakh granitoids derived from the different degree of interaction between metasomatized mantle derived mafic magmas mixing with felsic magmas of KLA lower crust (tonalite) and low to high K bearing Neotethyan oceanic amphibolite lower crust melting with least crustal melting of northern Indian metasediments (metapelites and metagreywackes) in the active southern margin of Ladakh batholiths (Fig. 8); [9,46]. The Nb/Ta ratio for mantle is 11.4 [50], whereas the mantle ratio is 17.8 [63], and the shallow crustal assimilation will result in the decreasing the Nb/Ta ratios [69]. The Nb/Ta (3.35-29.7) and Zr/Hf (13.8-42.0) values for the Ladakh granitoids in comparison with the average continental crust (Nb/Ta = 11; Zr/Hf = 33) suggesting that the mantle-crustal-derived magmas mixing processes [34]. The Ladakh granitoids have low Nb/Th (0.22-4.41) and Zr/Nb (0.19-6.62) represents the hydrous mantle derived mafic magmas with late-stage assimilation and magma mixing of granitic melts of crustal derived [40]. The assimilation of crustal materials enhances the Zr/Hf ratios. The high $(La/Yb)_N$ (1.6-36.4), Dy/Yb ratios (2.09-4.29) with flat HREE patterns for the Ladakh granitoids indicate the heterogeneous melting of source rocks with residual amphibole, garnet with or without plagioclase [15]. The negative correlations between CaO, TiO_2, Al_2O_3, Fe_2O_3, MgO, P_2O_5, and SiO_2 suggest that the Ladakh granitoids underwent mineral fractionations such as plagioclase, K-feldspar, Fe-Ti oxides, amphibole, biotite and apatite (Fig. 9), [1,34].
In summary, the Ladakh granitoids in the southern margin of Ladakh batholiths were generated by the subducted slab derived fluids/melts modified lithospheric mantle derived differentiated mafic magmas with late-stage assimilation, magmas mixing with felsic magmas of the heterogeneous partial melting of low to high K Neotethyan amphibolite lower crust, KLA tonalitic lower crust together with the northern Indian margin metasediments with residual amphibole, garnet with or without plagioclase derived.

5.3 Petrogenetic correlation between mafic enclaves and Ladakh granitoids

The linear trends between the mafic enclaves and host Ladakh granitoids on the Harker diagram and hyperbolic mixing arrays and linear trends observed between felsic host and MMEs in the major and tracer elemental variation diagrams (Fig. 9; Fig. 10) support magma mixing process. The presence of mafic enclaves in Ladakh granitoids, petrography, geochemical signature in mafic enclaves and Ladakh granitoids support the magma mixing/mingling processes (Fig. 2; Fig. 3; Fig. 5), [31,36].

5.4 Geodynamic implication

The enrichment of incompatible elements, low Nb/Ta ratios (< 2) and high Na_2O+K_2O (>5 wt.%) together with strong depletion HFSE (Nb, Ta, Zr, Hf), K suggest that the involvement of hydrous lithospheric mantle in the source region [4]. The mafic enclaves and Ladakh granitoids have high LREE, LILE with strong depletion in HFSE concentrations (Nb, Ta, Ti, P) and low HREE, which are typical characteristic of subduction-related magmatism [61,67,71]. Previous studies suggested that an Andean-style continental arc magmatisms in eastern Ladakh batholiths associated with northward subduction of Tethyan oceanic lithosphere on the southern margin of the Asia during the early Cretaceous to early Eocene, subsequent continental between India and Eurasian plates [21,54]. The subducted slab derived fluids/melts generates lithospheric mantle as well as enriched the lithospheric mantle [58]. The present study mafic enclaves and Ladakh granitoids plotted in volcanic arc field and post-collisional field represents the subduction of Neotethyan oceanic slab beneath the active margin of Kohistan Ladakh Arc lower crust of Eurasian plate, subsequent the post collisional processes such as slab roll-back induced the upwelling Neotethyan asthenospheric mantle upwelling and the initial contact between Indian and Eurasian plates (Fig. 11).

VI. Conclusion

- The subduction of Neotethyan oceanic slab roll-back generates overlying metasomatized Neotethyan lithospheric mantle in the southern active margin of Ladakh batholiths by oceanic slab/lithospheric mantle interaction.
- The field and petrographic studies exhibit the magma mixing process.
- The mafic enclaves and Ladakh granitoids form linear and hyperbolic trends in Harker diagram as well as major and tracer variations caused the magma mixing and mingling processes.
- The homogeneous tracer elemental patterns between mafic enclave and Ladakh granitoids indicates the attainment chemical equilibrium by the magma mixing processes
- The mafic enclaves formed by the subduction modified mantle source derived mafic magmas with intense fractional crystallization and late-stage assimilation of felsic magmas of Neotethyan amphibolite lower crustal melting.
- The I-type Ladakh granitoids were generated by mantle derived mafic mixing with felsic magmas of the heterogeneous melting of the heterogeneous source rocks of low to high K Neotethyan amphibolite lower crust, KLA tonalitic lower crust and northern Indian margin metasediments in the active margin of Eurasian plate.
- The formation of mafic enclaves and Ladakh granitoids related to the subducted Neotethyan slab roll-back induced asthenospheric mantle upwelling and the initial contact between Indian and Eurasian plates.

Reference

1. Ahmad, T.; Thakur, V.C.; Islam. R.; Khanna, P.P.; Mukherjee, P.K. Geochemistry and geodynamic implications of magmatic rocks from the trans-Himalayan arc. Geochemical Journal 1998, 32, 383–404.
2. Ahmad, T.; Harris, N.; Bickle, M.; Chapman, H.; Bunbury, J.; Prince, C. Isotopic constraints on the structural relationships between the lesser Himalayan series and the high Himalayan crystalline series, Garhwal Himalaya. Geological Society of America Bulletin 2000, 112(3), 467-477.
3. Ahmad, T.; Tanaka, T.; Sachan, H.K.; Asahara. Y.; Islam, R.; Khanna, P.P. Geochemical and isotopic constraints on the age and origin of the Nidar Ophiolitic Complex, Ladakh, India: implications for the Neo-Tethyan subduction along the Indus suture zone. Tectonophysics 2008, 451(1-4), 206-224.
4. Akbari, M.; Ghorbani, M.R.; Cousens, B.L.; Graham, I.T. Quaternary post-collisional high Nb-like basalts from Bijar-Qorveh, NW Iran: A metasomatized lithospheric mantle source. Lithos 2022, 426, 106781.
5. Allègre, C.J.; Ben Othman, D.B. Nd–Sr isotopic relationship in granitoid rocks and continental crust development: a chemical approach to orogenesis. Nature 1980, 286 (5771), 335-342.
6. Azizi, H.; Asahara, Y.; Minami, M.; Anma, R. Sequential magma injection with a wide range of mixing and mingling in Late Jurassic plutons, southern Ghorveh, western Iran. Journal of Asian Earth Sciences 2020, 200, 104469.
7. Barbarin, B. Mafic magmatic enclaves and mafic rocks associated with some granitoids of the central Sierra Nevada batholith, California: nature, origin, and relations with the hosts. Lithos 2005, 80 (1-4), 155-177.
8. Barbarin, B.; Didier, J. Genesis and evolution of mafic microgranular enclaves through various types of interaction between coexisting felsic and mafic magmas. Earth and Environmental Science Transactions of the Royal Society of Edinburgh 1992, 83(1-2), 145-153.
9. Bouilhol, P.; Jagoutz, O.; Hanchar, J.M.; Dudas, F.O. Dating the India–Eurasia collision through arc magmatic records. Earth Planetary Science Letter 2013, 366, 163–175.

10. Castro, A. The dual origin of I-type granites: the contribution from experiments. Geological Society of London, Special Publications 2020, 491 (1), 101-145.
11. Chappell, B.W.; Bryant, C.J.; Wyborn, D. Peraluminous I-type granites. Lithos 2012, 153, 142-153.
12. Chappell, B.W.; White, A.J. Two contrasting granite types: 25 years later. Australian journal of earth sciences 2001, 48(4), 489-499.
13. de Sigoyer, J.; Chavagnac, V.; Blichert-Toft, J.; Villa, I.M.; Luais, B.; Guillot, S.; Cosca, M.; Mascle, G. Dating the Indian continental subduction and collisional thickening in the northwest Himalaya: multichronology of the Tso Morari eclogites. Geology 2000, 28, 487-490.
14. DeCelles, P.G.; Robinson, D.M.; Zandt, G. Implications of shortening in the Himalayan fold-thrust belt for uplift of the Tibetan Plateau. Tectonics 2002, 21 (6), 12-1.
15. Defant, M.J.; Drummond, M.S. Derivation of some modern arc magmas by melting of young subducted lithosphere. Nature 1990, 347(6294), 662-665.
16. Dokuz, A. A slab detachment and delamination model for the generation of Carboniferous high-potassium I-type magmatism in the Eastern Pontides, NE Turkey: The Köse composite pluton. Gondwana Research 2011, 19(4), 926-944.
17. Frost, B.R.; Barnes, C.G.; Collins, W.J.; Arculus, R.J.; Ellis, D.J.; Frost, C.D. A geochemical classification for granitic rocks. Journal of petrology 2001, 42 (11), 2033-2048.
18. Gao, X.; Yu, S.; Li, S.; Santosh, M.; Liu, Y.; Jiang, X.; Peng, Y.; Zhao, S.; Lv, P. Syn-collisional I-type granitoids linked to lateral lithospheric heterogeneity: A case study from the North Qaidam orogen, NW China. Journal of Asian Earth Sciences 2022, 237, 105363.
19. Guillot, S.; De Sigoyer, J.; Lardeaux, J.M.; Mascle, G. Eclogitic metasediments from the Tso Morari area (Ladakh, Himalaya): Evidence for continental subduction during India-Asia convergence. Contributions to Mineralogy and Petrology 1997, 128 (2), 197-212.
20. Guillot, S.; Replumaz, A.; Hattori, K.H.; Strzerzynski, P. Initial geometry of western Himalaya and ultrahigh-pressure metamorphic evolution. Journal of Asian Earth Sciences 2007, 30 (3-4), 557-564.
21. Heri, A.R.; Aitchison, J.C.; King, J.A.; Villa, I.M. Geochronology and isotope geochemistry of Eocene dykes intruding the Ladakh Batholith. Lithos 2015; 212, 111-121.
22. Honegger. K.; Dietrich, V.; Frank, W.; Gansser, A.; Thöni, M.; Trommsdorff, V. Magmatism and metamorphism in the Ladakh Himalayas (the Indus-Tsangpo suture zone). Earth Planetary Science Letter 1982, 60 253-292.
23. Jiang, Y.H.; Jia, R.Y.; Liu, Z.; Liao, S.Y.; Zhao, P.; Zhou, Q. Origin of Middle Triassic high-K calc-alkaline granitoids and their potassic microgranular enclaves from the western Kunlun orogen, northwest China: A record of the closure of Paleo-Tethys. Lithos 2013, 156, 13-30.
24. Jiang, Z.Q.; Wang, Q.; Wyman, D.A.; Li, Z.X.; Yang, J.H.; Shi, X.B.; Ma, L.; Tang, G.J.; Gou, G.N.; Jia, X.H.; Guo, H.F. Transition from oceanic to continental lithosphere subduction in southern Tibet: Evidence from the Late Cretaceous–Early Oligocene (~ 91–30 Ma) intrusive rocks in the Chanang–Zedong area, southern Gangdese. Lithos 2014, 196, 213-231.
25. Kingson, O.; Bhutani, R.; Dash, J.K.; Sebastian, S.; Balakrishnan, S. Resolving the conundrum in origin of the Manipur Ophiolite Complex, Indo-Myanmar range: Constraints from Nd isotopic ratios and elemental concentrations in serpentinized peridotite. Chemical Geology 2017, 460, 117-129.
26. Kirstein, L.A. Thermal evolution and exhumation of the Ladakh Batholith, northwest Himalaya, India. Tectonophysics 2011, 503 (3-4), 222-233.
27. Koua, K.A.D.; Sun, H.; Li, J.; Li, H.; Xie, J.; Sun, Q.; Li, Z.; Yang, H.; Zhang, L.; Mondah, O.R. Petrogenesis of Early Cretaceous granitoids and mafic enclaves from the Jiaodong Peninsula, eastern China: Implications for crust-mantle interaction, tectonic evolution and gold mineralization. Journal of Asian Earth Sciences 2022, 228, 105096.
28. Kumar, S. Mafic to hybrid microgranular enclaves in the Ladakh batholith, northwest Himalaya: Implications on calc-alkaline magma chamber processes. Journal of the Geological Society of India 2010, 76 (1), 5-25.
29. Kumar, S. Schedule of mafic to hybrid magma injections into crystallizing felsic magma chambers and resultant geometry of enclaves in granites: new field and petrographic observations from Ladakh Batholith, Trans-Himalaya, India. Frontiers in Earth Science 2020; 8, 551097.
30. Kumar, S.; Rino, V. Mineralogy and geochemistry of microgranular enclaves in Palaeoproterozoic Malanjkhand granitoids, central India: evidence of magma mixing, mingling, and chemical equilibration. Contributions to Mineralogy and Petrology 2016, 152 (5), 591-609.
31. Langmuir, C.H.; Vocke, Jr.; R.D.; Hanson, G.N.; Hart, S.R. A general mixing equation with applications to Icelandic basalts. Earth and Planetary Science Letters 1978, 37 (3), 380-392.

32. Laurent, O.; Martin, H.; Moyen, J.F.; Doucelance, R. The diversity and evolution of Late-Archean granitoids: Evidence for the onset of "modern-style" plate tectonics between 3.0 and 2.5 Ga. Lithos 2014, 205, 208-235.
33. Leat, P.T.; Livermore, R.A.; Millar, I.L.; Pearce, J.A. Magma supply in back-arc spreading centre segment E2, East Scotia Ridge. Journal of Petrology 2000, 41(6), 845-866.
34. Liu, X.Q.; Zhang, C.L.; Hao, X.S.; Zou, H.; Zhao, H.X.; Ye, X.T. Early Cretaceous granitoids in the Southern Pamir: Implications for the Meso-Tethys evolution of the Pamir Plateau. Lithos 2020, 362, 105492.
35. Liu, Z.; Jiang, Y.H.; Jia, R.Y.; Zhao, P.; Zhou, Q. Origin of Late Triassic high-K calc-alkaline granitoids and their potassic microgranular enclaves from the western Tibet Plateau, northwest China: Implications for Paleo-Tethys evolution. Gondwana Research 2015, 27(1), 326-341.
36. Ma, X.; Meert, J.G.; Xu, Z.; Zhao, Z. Evidence of magma mixing identified in the Early Eocene Caina pluton from the Gangdese Batholith, southern Tibet. Lithos 2017, 278, 126-139.
37. Mahéo, G.; Bertrand, H.; Guillot, S.; Villa, I.M.; Keller, F.; Capiez, P. The South Ladakh ophiolites (NW Himalaya, India): an intra-oceanic tholeiitic arc origin with implication for the closure of the Neo-Tethys. Chemical geology 2004, 203 (3-4), 273-303.
38. Maniar, P.D.; Piccoli, P.M. Tectonic discrimination of granitoids. Geological society of America bulletin 1989, 101(5), 635-643.
39. Middlemost, E.A. Naming materials in the magma/igneous rock system. Earth-science reviews 1994, 37(3-4), 215-224.
40. Moradi, S.; Jiang, S.Y.; Christiansen, E.H.; Ghorbani, M.R. Petrogenesis of Tertiary granitoid rocks from east of the Bidhand fault, Urumieh-Dokhtar Magmatic Arc, Iran: Implication for an active continental margin setting. Lithos 2021, 400, 106422.
41. Patiño Douce, A.E. What do experiments tell us about the relative contributions of crust and mantle to the origin of granitic magmas? Geological Society of London Special. Publications 1999, 168, 55–75.
42. Pearce, J.A.; Harris, N.B.W.; Tindle, A.G. Trace element discrimination diagrams for the tectonic interpretation of granitic rocks. Journal Petrology 1984, 25, 956–983.
43. Pearce, J.A.; Peate, D.W. Tectonic implications of the composition of volcanic arc magmas. Annual review of Earth and planetary sciences 1995, 23, 251-286.
44. Peate, D.W.; Pearce, J.A.; Hawkesworth, C.J.; Colley, H.; Edwards, C.M.; Hirose, K. Geochemical variations in Vanuatu arc lavas: the role of subducted material and a variable mantle wedge composition. Journal of Petrology 1997, 38(10), 1331-1358.
45. Pitcher, W.S. Granites and yet more granites forty years on. Geologische Rundschau 1987, 76(1), 51-79.
46. Ravikant, V.; Wu, F.Y.; Ji, W.Q. Zircon U–Pb and Hf isotopic constraints on petrogenesis of the Cretaceous–Tertiary granites in eastern Karakoram and Ladakh, India. Lithos 2009, 110(1-4), 153-166.
47. Reichardt, H.; Weinberg, R.F.; Andersson, U.B.; Fanning, C.M. Hybridization of granitic magmas in the source: the origin of the Karakoram Batholith, Ladakh, NW India. Lithos 2010, 116 (3-4), 249-272.
48. Richards, A.; Argles, T.; Harris, N.; Parrish, R.; Ahmad, T.; Darbyshire, F.; Draganits, E. Himalayan architecture constrained by isotopic tracers from clastic sediments. Earth and Planetary Science Letters 2005, 236 (3-4), 773-796.
49. Rolland, Y.; Picard, C.; Pecher, A.; Lapierre, H.; Bosch, D.; Keller, F. The Cretaceous Ladakh arc of NW Himalaya—slab melting and melt–mantle interaction during fast northward drift of Indian Plate. Chemical Geology 2002, 182, 139–178.
50. Rudnick, R.L.; Gao, S.; Holland, H.D.; Turekian, K.K. Composition of the continental crust. The crust 2003, 3, 1-64.
51. Sachan, H.K. Cooling history of subduction related granite from the Indus Suture zone, Ladakh, India: evidence from fluid inclusions. Lithos 1996, 38 (1-2), 81-92.
52. Saini, N.K.; Mukherjee, P.K.; Rathi, M.S.; Khanna, P.P. Evaluation of energy-dispersive x-ray fluorescence spectrometry in the rapid analysis of silicate rocks using pressed powder pellets. X-Ray Spectrometry: An International Journal 2000, 29 (2), 166-172.
53. Saini, N.K.; Mukherjee, P.K.; Rathi, M.S.; Khanna, P.P.; Purohit, K.K. Trace element estimation in soils: an appraisal of ED-XRF technique using group analysis scheme. Journal of Trace and Microprobe Techniques 2002, 20(4), 539-551.
54. Saktura, W.M.; Buckman, S.; Aitchison, J.C.; Zhou, R. Paleogene magmatic flex and flux in the Ladakh Arc, NW Himalaya: Chronostratigraphy of the Khardung Formation. Lithos 2021, 388, 106053.
55. Sargazi, M.; Bagheri, S.; Ma, X. Oligocene calc-alkaline lamprophyres and K-rich association in the eastern Iranian ranges: Products of low-degree melting of subduction-modified lithospheric mantle in post-orogenic setting. Lithos 2022, 430, p.106864.

56. Schannor, M.; Lana, C.; Mazoz, A.; Narduzzi, F.; Cutts, K.; Fonseca, M. Paleoproterozoic sources for Cordilleran-type Neoproterozoic granitoids from the Araçuaí orogen (SE Brazil): Constraints from Hf isotope zircon composition. Lithos 2020, 378, 105815.
57. Schärer, U.; Hamet, J.; Allègre, C.J. The Transhimalaya (Gangdese) plutonism in the Ladakh region: a UPb and Rb-Sr study. Earth and Planetary Science Letters 1984, 67(3), 327-339.
58. Shellnutt, J.G.; Lee, T.Y.; Brookfield, M.E.; Chung, S.L. Correlation between magmatism of the Ladakh batholith and plate convergence rates during the India–Eurasia collision. Gondwana Research 2014, 26, 1051–1059.
59. Singh, S.; Kumar, R.; Barley, M.E.; Jain, A.K. Shrimp U–Pb ages and depth of emplacement of Ladakh batholith, Eastern Ladakh, India. Journal Asian Earth Science 2007; 30, 490–503.
60. Spencer, C.J.; Dyck, B.; Mottram, C.M.; Roberts, N.M.; Yao, W.H.; Martin, E.L. Deconvolving the pre-Himalayan Indian margin–tales of crustal growth and destruction. Geoscience Frontiers 2019, 10(3), 863-872.
61. Stern, R.J. Subduction zones. Reviews of geophysics 2002, 40(4), 3-1.
62. St-Onge, M.R.; Rayner, N.; Searle, M.P. Zircon age determinations for the Ladakh batholith at Chumathang (Northwest India): implications for the age of the India–Asia collision in the Ladakh Himalaya. Tectonophysics 2010; 495(3-4), 171-183.
63. Sun, S.S.; McDonough, W.F. Chemical and isotopic systematics of oceanic basalts: implications for mantle composition and processes. Geological Society of London, Special Publications 1989, 42(1), 313-345.
64. Thanh, N.X.; Itaya, T.; Ahmad, T.; Kojima, S.; Ohtani, T.; Ehiro, M. Mineral chemistry and K–Ar ages of plutons across the Karakoram fault in the Shyok-Nubra confluence of northern Ladakh Himalaya, India. Gondwana Research 2010, 17(1), 180-188.
65. Thanh, N.X.; Rajesh, V.J.; Itaya, T.; Windley, B.; Kwon, S.; Park, C.S. A Cretaceous forearc ophiolite in the Shyok suture zone, Ladakh, NW India: Implications for the tectonic evolution of the Northwest Himalaya. Lithos 2012, 155, 81-93.
66. Thie´blemont, D., Tegyey, M., 1994. Une discrimination ge´ochimique des roches diffe´rencie´es te´moin de la diversite´ d'origine et de situation tectonique des magmas calco-alcalins. C.R. Acad. Sci. Paris 319 (II), 87–94
67. Upadhyay, R.; Frisch, W.; Siebel, W. Tectonic implications of new U–Pb zircon ages of the Ladakh batholith, Indus suture zone, northwest Himalaya, India. Terra Nova 2008, 20, 309–317.
68. Walsh, J.M.; Buckman. S.; Nutman, A.P.; Zhou, R. The significance of Upper Jurassic felsic volcanic rocks within the incipient, intraoceanic Dras Arc, Ladakh, NW Himalaya. Gondwana Research 2021, 90, 199-219.
69. Wang, Z.; Zhao, Z.; Asimow, P.D.; Li, X.; Meng, Y.; Liu, D.; Mo, X.; Zhu, D.C.; Tang, Y.; Cong, F. Two episodes of Eocene mafic magmatism in the southern Lhasa terrane imply an eastward propagation of slab breakoff. Gondwana Research 2022, 110, 31-43.
70. Weinberg, R.F.; Dunlap, W.J. Growth and deformation of the Ladakh batholith, Northwest Himalayas: implications for timing of continental collision and origin of calc-alkaline batholiths. Journal of Geology 2000, 108, 303–320
71. White, L.T.; Ahmad, T.; Ireland, T.R.; Lister, G.S.; Forster, M.A. Deconvolving episodic age spectra from zircons of the Ladakh batholith, northwest Indian Himalaya. Chemical Geology 2011, 289, 179–196.
72. White, L.T.; Ahmad, T.; Lister, G.S.; Ireland, T.R.; Forster, M.A. Is the switch from I-to S-type magmatism in the Himalayan Orogen indicative of the collision of India and Eurasia? Australian Journal of Earth Sciences 2012, 59(3), 321-340.
73. Yan, M.; Wei, J.; Zhang, D.; Zhao, Z.; Turlin, F.; Li, H.; Li, G.; Xu, C.; Zhang, X.; Moritz, R. Petrogenesis of Late Devonian I-and A-type granitoids, and associated mafic microgranular enclaves in the northwestern North Qaidam Orogenic Belt, China: Implications for continental crust growth during the post-collisional stage. Lithos 2022, 430, 106857.
74. Yang, Z.Y.; Wang, Q.; Yang, J.H.; Dan, W.; Zhang, X.Z.; Ma, L.; Qi, Y.; Wang, J.; Sun, P. Petrogenesis of Early Cretaceous granites and associated microgranular enclaves in the Xiabie Co area, central Tibet: Crust-derived magma mixing and melt extraction. Lithos 2019, 350, 105199.

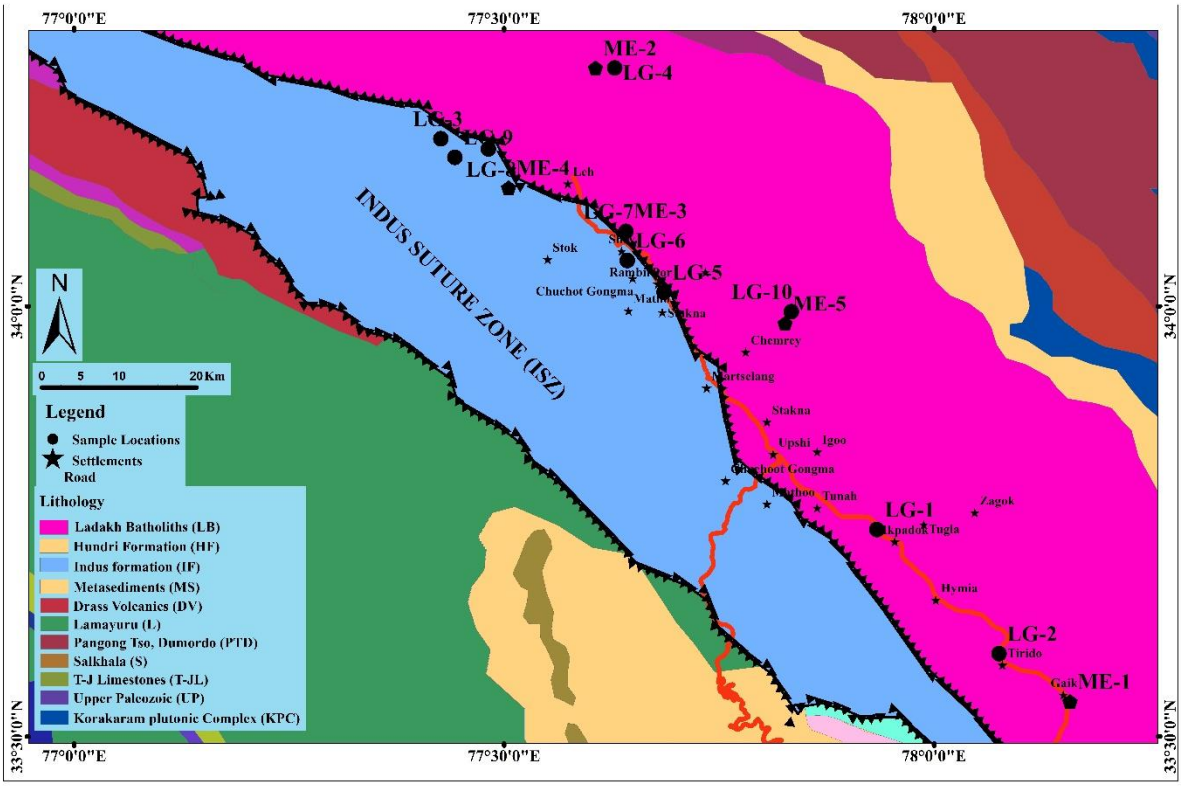

Fig 1. Simplified geological and sample location map in the southern margin of granitoids of Ladakh batholith, Indus Suture zone.

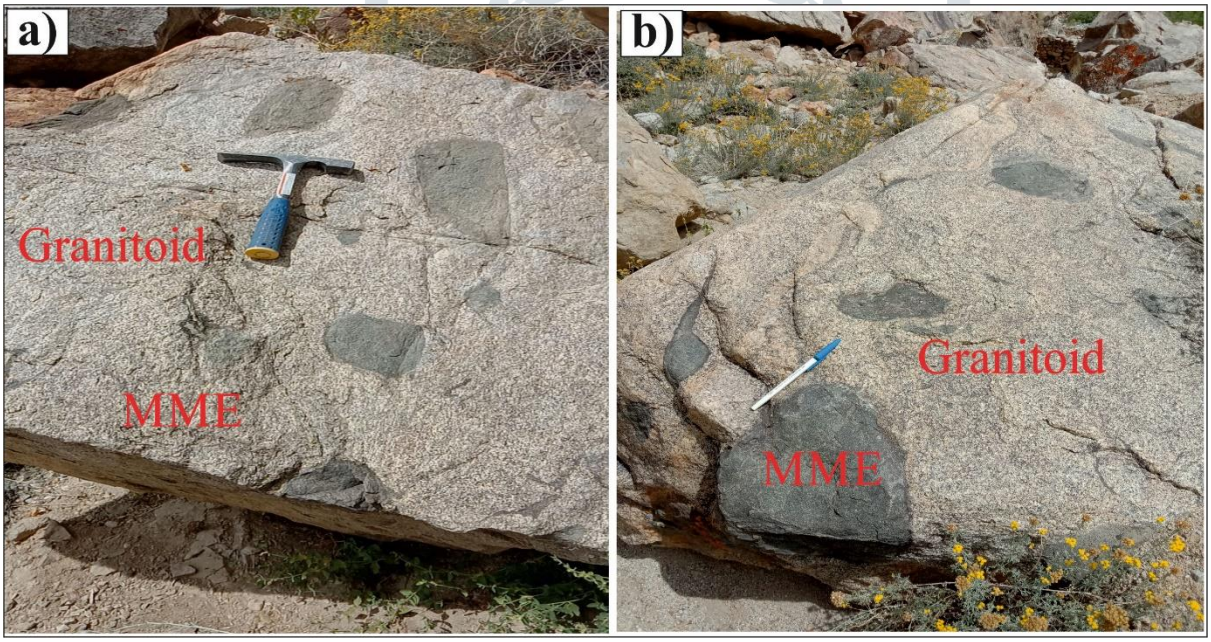

Fig 2. Field photographs of mafic enclave-Ladakh granitoid relationship in the southern margin of granitoid of Ladakh batholiths (a-b) spherical, globular, tabular to elongated mafic enclaves with sharp contact with its porphyritic host Ladakh granitoids.

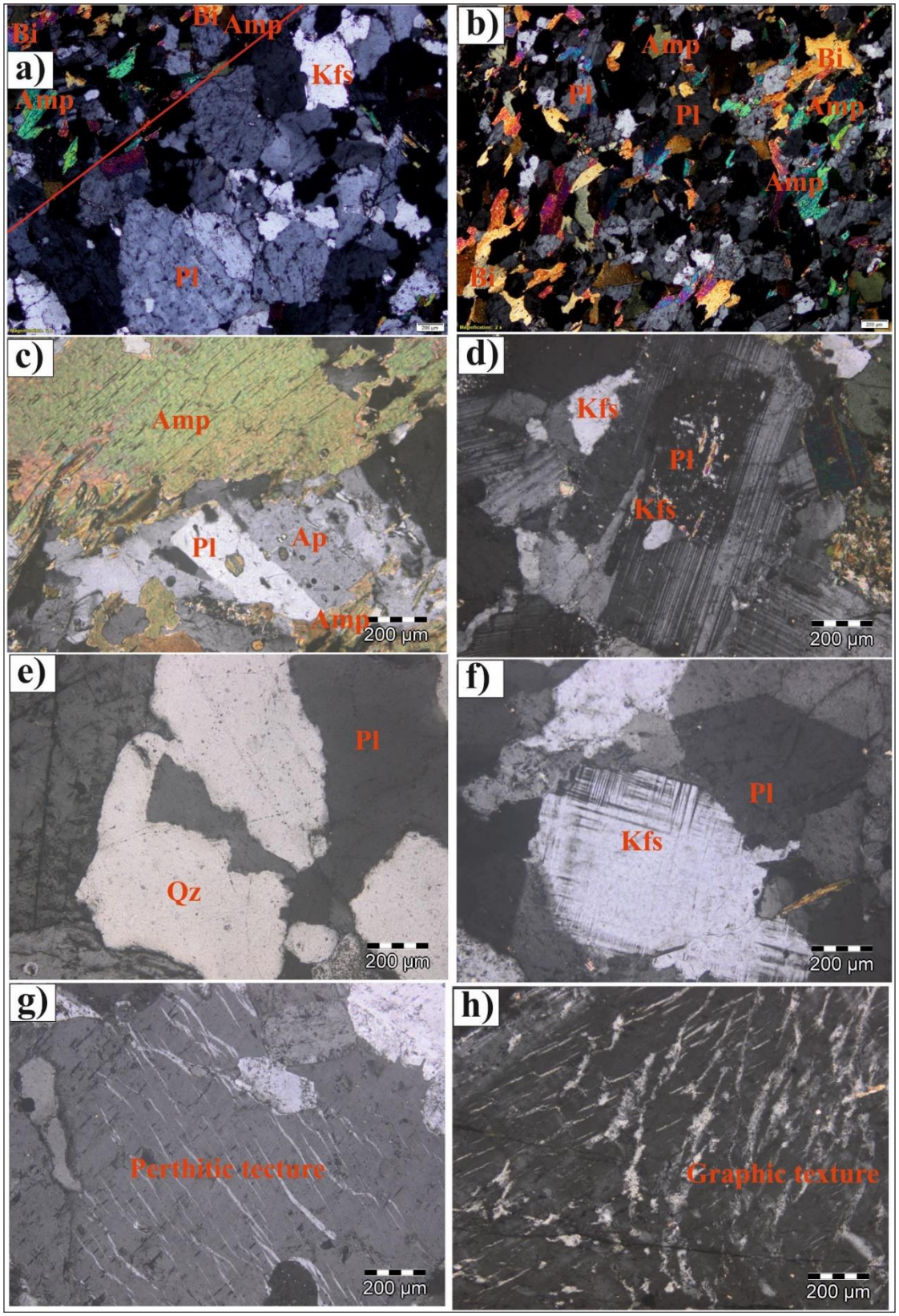

Fig 3. Petrographic observation in mafic enclaves (a) The mafic enclave and granitoids mixing; (b) magmatic flow texture of plagioclase, amphibole and biotite in mafic enclave; (c) amphibole megacryst and acicular apatite; (d) plagioclase megacryst with resorbed core. Petrographic observation in Ladakh granitoids (e) the growth of apatite megacryst within plagioclase; (f) K-feldspar surrounded by plagioclase; (g-h) perthitic and graphic textures in plagioclase

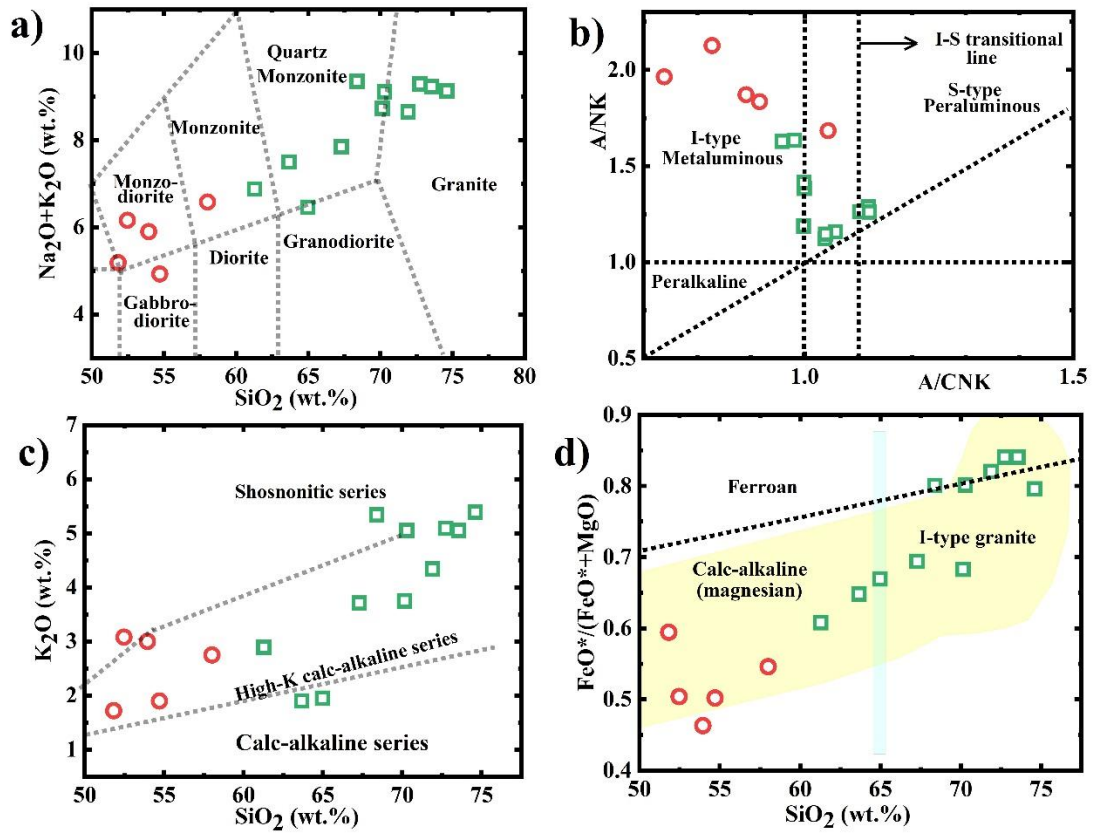

Fig 4. Discrimination diagram for the mafic enclave and Ladakh granitoids (a) SiO_2 versus (K_2O+Na_2O) after Middlemost, (1994); (b) SiO_2 versus K_2O after Maniar and Picooli, (1989); (c) Alumina saturation index (A/CNK [molar Al_2O_3/(CaO+Na_2O+K_2O]) versus A/NK plot after Frost et al., (2001); (d) FeO*/(FeO*+MgO) versus SiO_2 plot after Castro, (2020). The symbols for mafic enclaves and Ladakh granitoids are the same in all figures, except Figure 6.

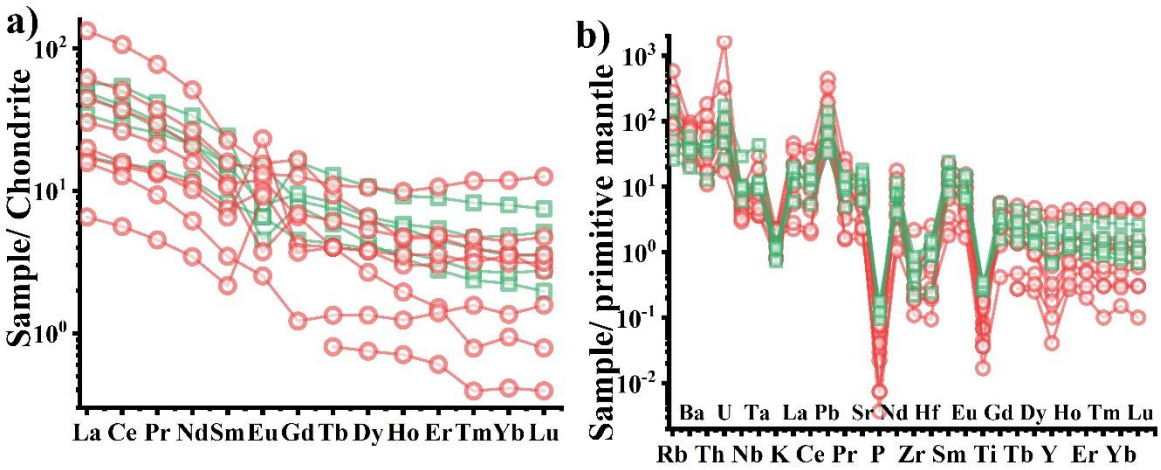

Fig 5. Normalized diagrams for mafic enclave and Ladakh granitoids (a) chondrite normalized diagram; (b) primitive mantle normalized spider diagram. The normalized data are from Sun and McDonough, (1989).

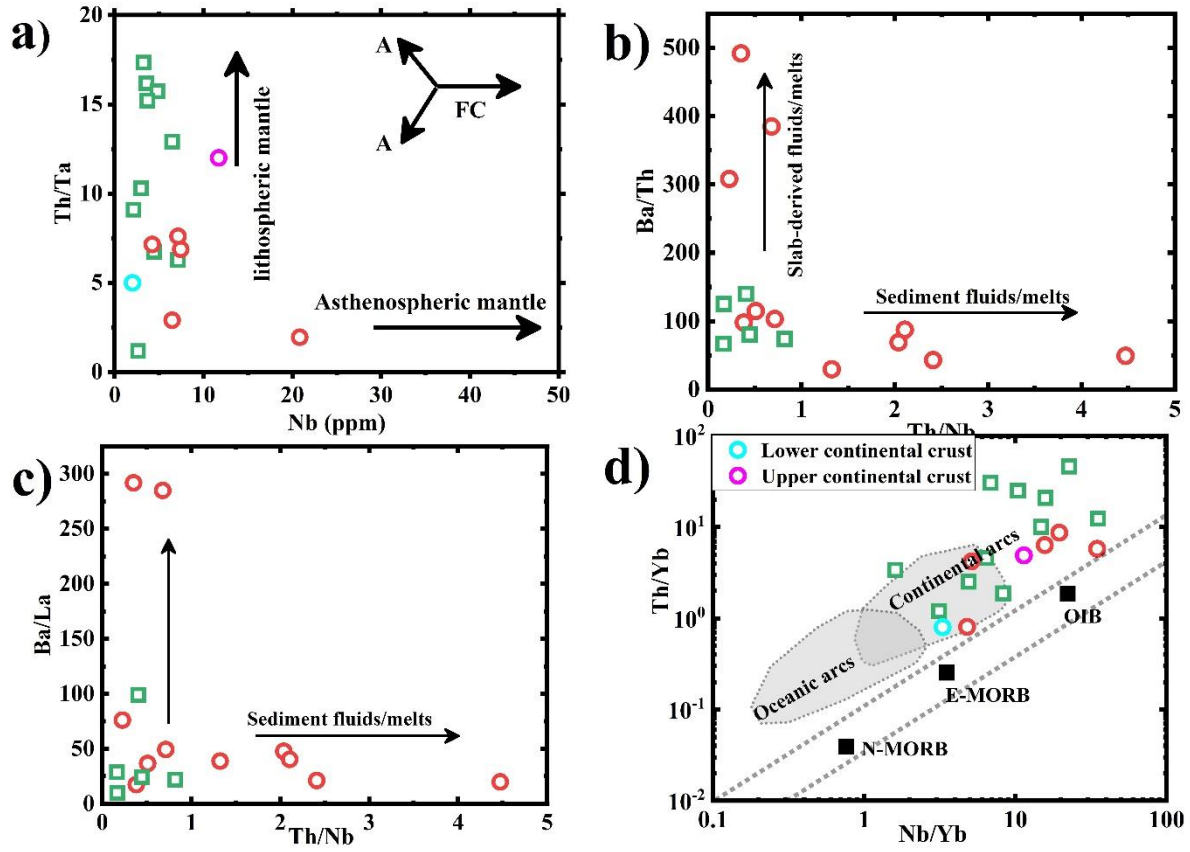

Fig 6. Th/Ta versus Nb after Akbari et al., (2022); (b) Ba/Th versus Th/Nb after Leat et al., (2000); (c) Ba/La versus Th/Nb after Dokuz, (1997); (d) Th/Yb versus Nb/Yb after Pearce and Peate, (1995). A- Assimilation; FC- Fractional crystallization.

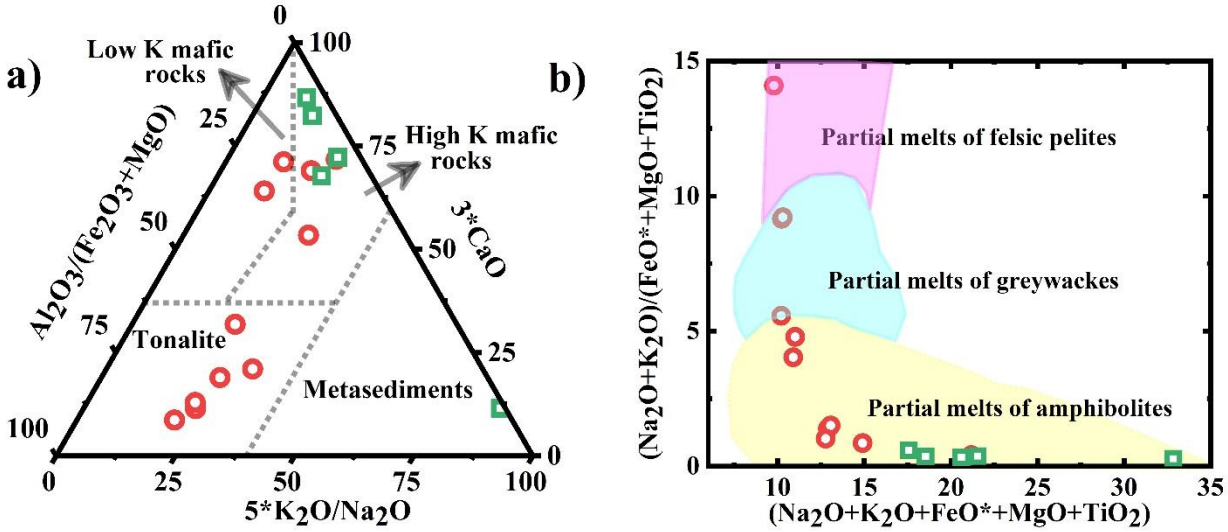

Fig 7. The source discrimination diagram (a) $5*K_2O/Na_2O$-$3*CaO$- $Al_2O_3/(FeO*+MgO)$ ternary diagram after Laurent et al., (2014); (b) $(Na_2O+K_2O+FeO*+MgO+TiO_2)$ versus $(Na_2O+K_2O)/(FeO*+MgO+TiO_2)$ after Patiño Douce, (1999).

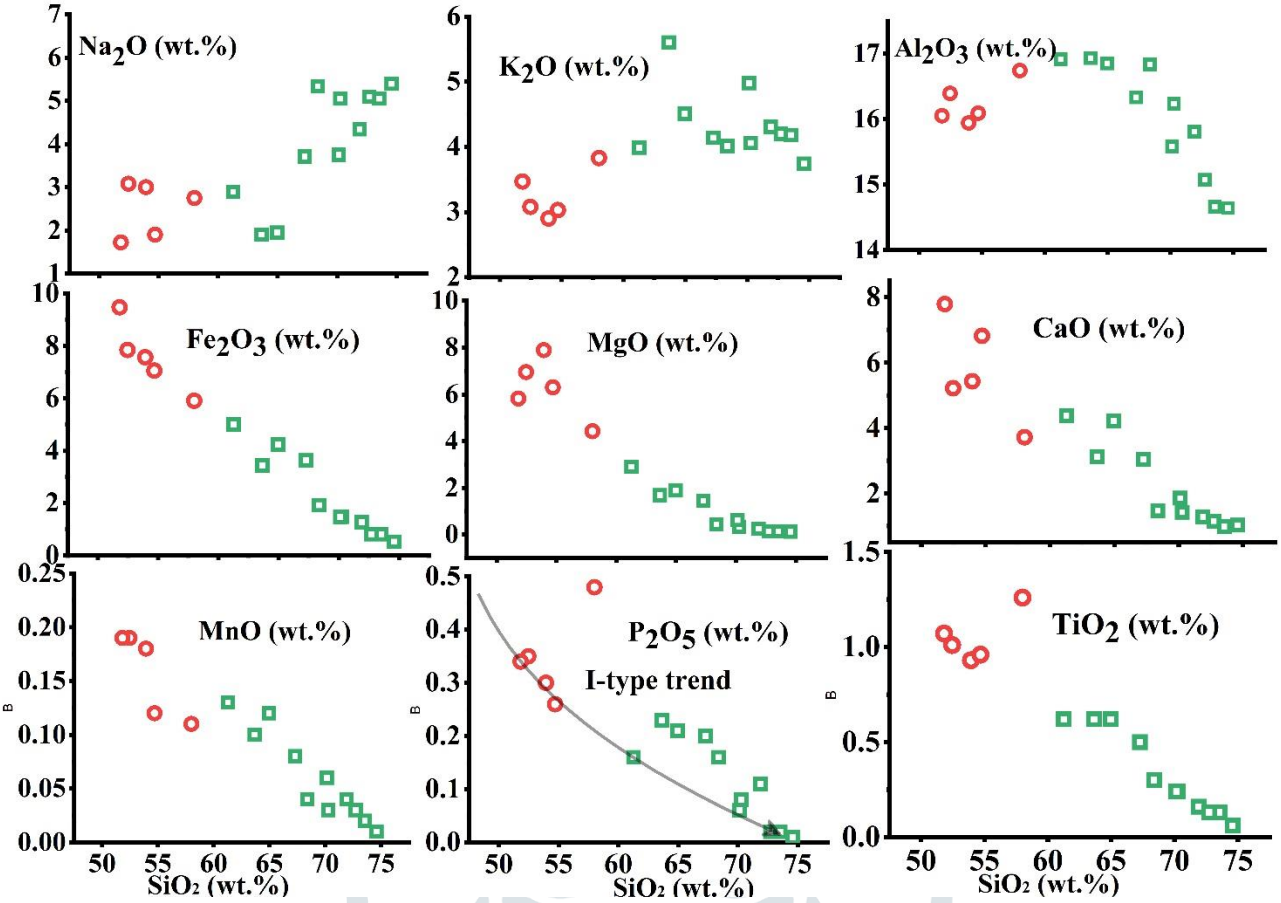

Fig 8. The major oxides plotted against SiO_2 for the mafic enclave and Ladakh granitoids.

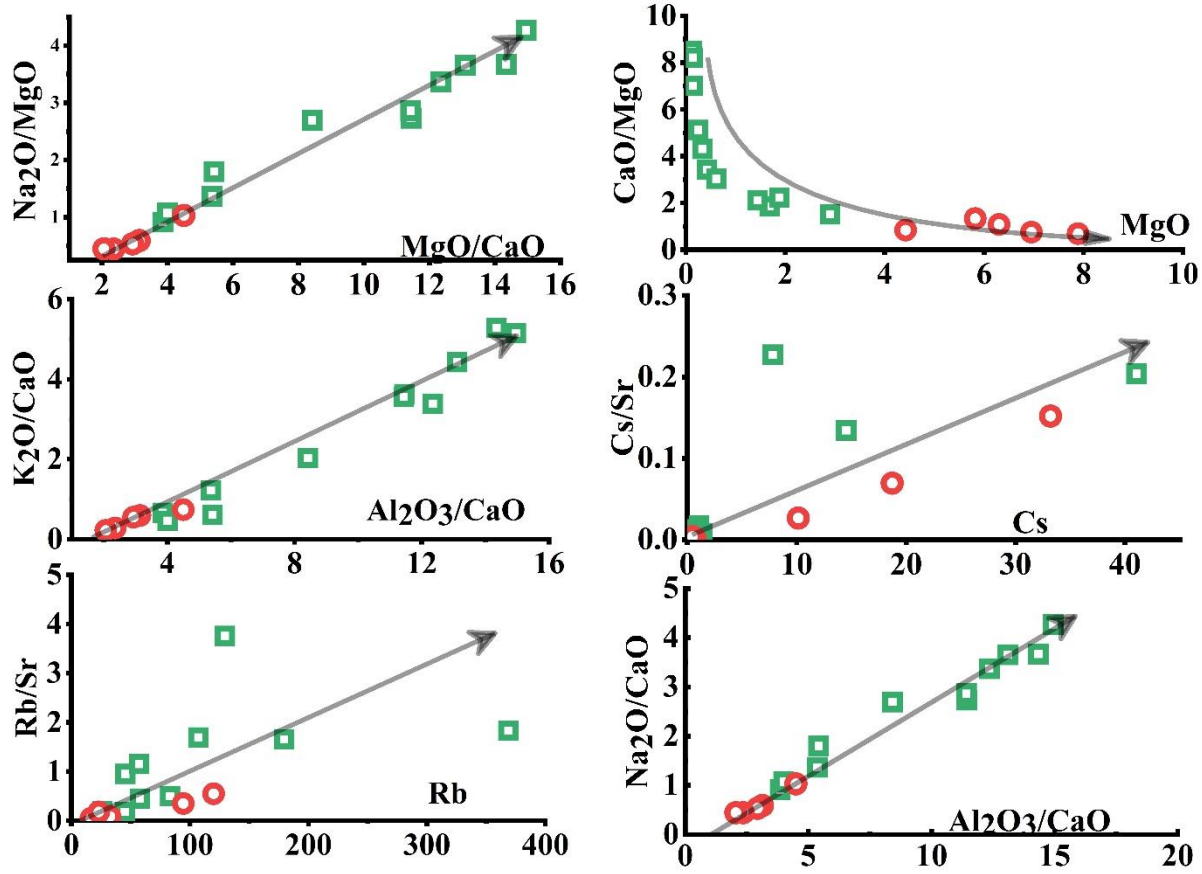

Fig 10. Geochemical correlation diagrams for the mafic enclaves and Ladakh granitoids (a) Na_2O/MgO versus MgO/CaO; (b) CaO/MgO versus MgO; (c) K2O/CaO versus Al_2O_3/CaO; (d) Cs/Sr versus Sr; (e) Rb/Sr versus Rb; (e) Na_2O/CaO versus Al_2O_3/CaO after Longmuir et al., (1978).

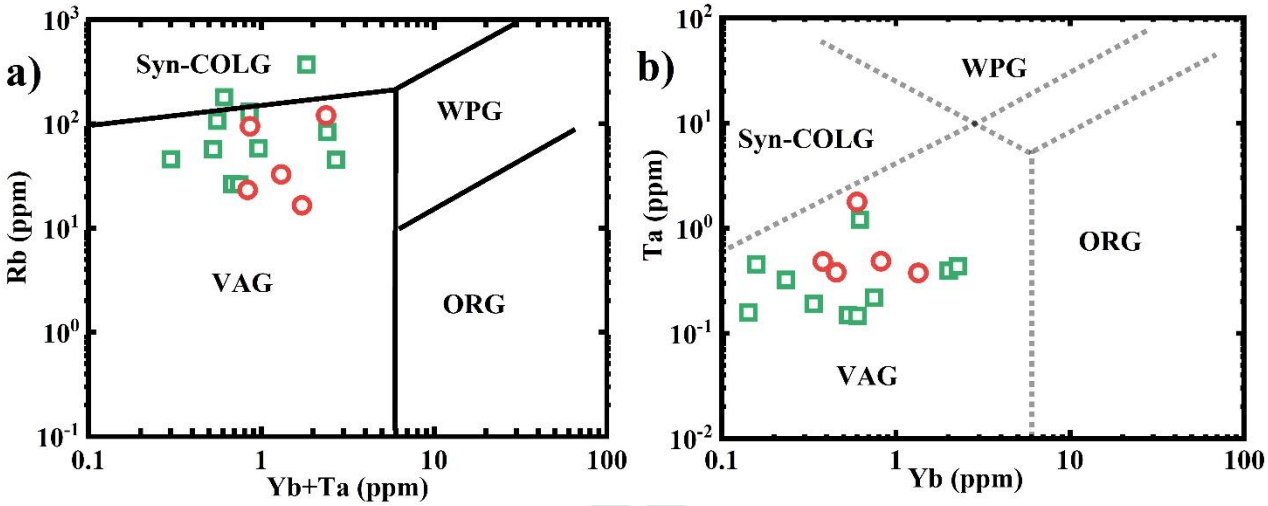

Fig 11. Tectonic discrimination diagram (a) Rb versus Yb+Ta; (b) Ta versus Yb after Pearce et al., (1984). VAG-Volcanic arc granites, Syn-COLG- Syn-collisional granites, WPG- Within-plate granites, ORG- Oceanic-ridge granites.

Table 1. Sample information for the mafic enclaves and Ladakh granitoids in the southern margin of Ladakh batholiths, Indus Suture zone.

S. No	Sample ID	Rock type	Latitude	Longitude	Mineral Assemblage
1.	LG-1	Tunah MME	33°44'25".6	77°56'00".76	Plagioclase, K-feldspar, Quartz, epidote, ilmenite
2.	LG-2	Ladakh Granitoids	33°35'46".2	78°04'32".6	Plagioclase-K-feldspar-Quartz-Zircon, apatite, magnetite, sphene
3.	LG-3		34°11'40".7	77°25'35".5	Plagioclase-K-feldspar-Quartz
4.	LG-4		34°16'37".5	77°37'43".5	Plagioclase-K-feldspar-Quartz
5.	LG-5		34°00'58".9	77°41'10".4	Plagioclase-K-feldspar-Quartz-biotite
6.	LG-6		34°03'11".6	77°38'36".2	Plagioclase-K-feldspar-Quartz-zircon, apatite
7.	LG-7		34°05'13".3	77°38'30".8	Plagioclase-K-feldspar-Quartz
8.	LG-8		34°10'58".1	77°28'54".5	Plagioclase-K-feldspar-Quartz-zircon-biotite
9.	LG-9		34°10'23".2	77°26'34".5	Plagioclase-K-feldspar-Quartz-biotite
10.	LG-10		33°59'37".2	77°50'02".6	Plagioclase-K-feldspar-Quartz
11.	LG-11		33°44'25".6	77°56'00".76	Plagioclase-K-feldspar-Quartz-muscovite
12.	ME-1	Mafic enclaves	33°32'25".6	78°09'29".7	Plagioclase, amphibole, biotite, titanite
13.	ME-2		34°16'37".4	77°36'22".9	Plagioclase, amphibole, biotite, magnetite, K-feldspar
14.	ME-3		34°05'15".8	77°38'30".8	Plagioclase, amphibole, biotite, apatite, quartz, K-feldspar
15.	ME-4		34°08'15".7	77°30'19".3	Plagioclase-K-feldspar-Quartz
16.	ME-5		33°58'48".4	77°49'36".3	Plagioclase, hornblende, biotite, quartz, titanite

Table 2. Major oxides (wt. %) and tracer element (ppm) results of mafic enclaves and Ladakh granitoids in the southern margin of Ladakh batholiths.

Sample ID	LG -1	LG-2	LG-3	LG-4	LG-5	LG-6	LG-7	LG-8	LG-9	LG-10	LG-11	ME-1	ME-2	ME-3	ME-4	ME-5
Type	Ladakh granitoids											Mafic enclaves				
SiO_2	68.38	70.28	70.14	63.66	61.27	67.28	74.59	71.90	64.97	73.55	72.73	52.46	53.94	54.70	51.82	58.01
TiO_2	0.30	0.24	0.24	0.62	0.62	0.50	0.06	0.16	0.62	0.13	0.13	1.01	0.93	0.96	1.07	1.26
Al_2O_3	16.83	16.23	15.58	16.93	16.91	16.33	14.64	15.81	16.85	14.66	15.07	16.39	15.94	16.09	16.05	16.74
Fe_2O_3	1.92	1.48	1.46	3.44	5.00	3.63	0.52	1.27	4.23	0.82	0.82	7.85	7.57	7.06	9.48	5.91
MnO	0.04	0.03	0.06	0.10	0.13	0.08	0.01	0.04	0.12	0.02	0.03	0.19	0.18	0.12	0.19	0.11
MgO	0.43	0.33	0.61	1.68	2.90	1.44	0.12	0.25	1.88	0.14	0.14	6.95	7.89	6.30	5.82	4.42
CaO	1.47	1.42	1.85	3.12	4.38	3.04	1.02	1.28	4.21	0.98	1.15	5.22	5.43	6.82	7.79	3.72
Na_2O	5.34	5.05	3.75	1.90	2.89	3.71	5.39	4.34	1.95	5.05	5.09	3.08	3.00	1.90	1.72	2.75
K_2O	4.01	4.06	4.98	5.60	3.99	4.14	3.74	4.31	4.51	4.18	4.20	3.08	2.90	3.03	3.47	3.83
P_2O_5	0.16	0.08	0.06	0.23	0.16	0.20	0.01	0.11	0.21	0.02	0.02	0.35	0.30	0.26	0.34	0.48
LOI	1.50	1.22	0.76	2.75	1.00	0.83	0.51	1.26	0.99	0.71	0.71	2.02	1.90	4.08	1.34	2.00
Total	98.88	99.20	98.73	97.28	98.25	100.3	100.1	99.47	99.55	99.55	99.38	96.58	98.08	97.24	97.75	97.23
A/CNK	1.12	1.10	1.00	1.00	0.96	1.00	1.06	1.12	0.98	1.04	1.04	0.92	0.89	0.83	0.74	1.04
Mg#	33	33	48	52	56	47	34	30	49	27	27	66	70	66	57	62
Sc	2.03	1.05	2.71	1.76	4.03	2.67	0.80	2.77	8.17	0.65	0.68	9.81	4.85	11.31	9.87	2.77
V	21.75	11.85	12.57	32.04	102.2	57.67	2.87	4.81	72.63	2.96	2.92	118.50	139.51	198.8	215.4	54.13
Cr	0.54	1.64	1.00	1.14	8.42	7.01	0.09	1.76	3.26	0.39	0.53	80.54	118.69	28.88	15.21	5.40
Co	96.61	152.45	149.9	98.13	105.5	100.2	152.6	152.0	95.87	131.36	131.59	59.74	84.51	81.59	64.61	107.8
Ni	0.22	0.73	0.11	0.12	3.76	3.01	0.00	0.23	1.25	0.00	0.32	38.16	50.52	10.16	12.90	2.70
Cu	2.09	2.32	0.84	1.09	5.42	5.87	0.72	3.71	4.88	0.81	0.06	27.29	7.57	7.64	10.61	16.30
Zn	1143	1600	1359	1945	1626	1904	2188	1814	1469	1678	1144	1286	1467	1358	1715	1197
Ga	26.00	19.87	17.76	15.68	12.81	14.75	9.60	17.82	13.75	14.42	13.27	19.92	15.37	13.91	13.08	15.24
Ge	0.59	0.38	0.47	0.64	0.84	0.69	0.31	0.35	0.71	0.40	0.37	1.04	0.87	0.94	1.12	0.96
Rb	368.67	179.61	83.23	26.34	26.07	58.02	106.9	129.6	44.90	45.57	56.88	120.04	94.49	32.61	16.48	23.17
Sr	201.54	108.28	164.9	182.5	132.9	128.6	63.08	34.48	248.06	47.74	49.40	218.61	270.11	381.3	336.4	129.6
Y	5.67	1.09	13.61	2.79	3.50	4.98	0.81	0.19	18.48	0.46	1.49	6.25	3.22	7.52	11.04	3.05
Zr	1.23	2.15	3.35	3.19	5.48	5.32	24.45	7.08	6.68	2.48	2.07	3.99	4.75	7.16	9.56	2.43
Nb	6.46	3.58	3.23	4.42	2.96	4.80	3.70	2.62	7.10	2.10	2.31	20.82	7.43	4.21	6.45	7.12
Mo	0.00	0.00	0.11	0.00	0.00	0.00	0.00	0.00	0.00	0.00	0.00	0.00	0.00	0.09	0.00	0.00
Cd	0.03	0.01	0.04	0.02	0.03	0.05	0.04	0.04	0.06	0.00	0.01	0.09	0.08	0.04	0.09	0.01

Cs	41.08	14.54	1.16	1.38	0.70	0.82	1.08	7.83	0.83	0.52	0.62	33.19	18.73	10.15	0.70	0.48
Ba	670.98	504.44	595.2	309.1	173.6	353.7	145.4	453.3	265.97	550.21	509.06	231.82	266.09	254.9	136.3	404.9
La	31.52	10.55	14.70	4.06	4.73	7.15	3.74	1.55	15.14	1.93	25.48	8.08	10.96	11.61	13.58	4.09
Ce	65.10	22.63	30.88	9.12	9.69	16.03	7.78	3.43	34.17	3.85	53.83	17.63	22.52	24.40	33.24	9.50
Pr	7.34	2.80	3.54	1.25	1.28	2.03	0.89	0.43	3.93	0.46	5.64	2.42	2.64	2.91	3.95	1.36
Nd	23.87	9.56	12.34	5.29	4.75	7.37	2.87	1.61	14.60	1.44	17.70	9.86	10.04	11.19	15.70	5.57
Sm	3.46	1.72	2.44	1.14	1.00	1.64	0.53	0.33	3.35	0.28	2.16	2.35	1.95	2.33	3.70	1.26
Eu	0.58	0.26	0.69	0.53	0.25	0.32	0.15	0.10	0.90	0.22	0.38	0.39	0.46	0.76	0.86	0.38
Eu	0.66	0.31	0.73	0.57	0.26	0.36	0.16	0.15	0.90	0.28	0.39	0.40	0.47	0.73	0.77	0.39
Gd	3.41	1.35	2.61	0.86	0.76	1.42	0.25	-0.04	3.28	0.00	2.26	1.75	1.61	1.95	3.29	0.93
Tb	0.35	0.15	0.41	0.15	0.15	0.23	0.05	0.03	0.55	0.03	0.18	0.28	0.22	0.31	0.48	0.16
Dy	1.67	0.68	2.68	0.96	0.96	1.35	0.34	0.19	3.51	0.24	0.70	1.53	1.09	1.66	2.72	1.00
Ho	0.26	0.11	0.56	0.17	0.20	0.27	0.07	0.04	0.73	0.05	0.12	0.31	0.19	0.33	0.52	0.21
Er	0.78	0.25	1.76	0.50	0.59	0.81	0.23	0.10	2.18	0.14	0.40	0.74	0.46	0.90	1.48	0.54
Tm	0.10	0.02	0.30	0.09	0.08	0.12	0.04	0.01	0.33	0.02	0.04	0.10	0.06	0.12	0.21	0.07
Yb	0.62	0.16	2.01	0.53	0.60	0.75	0.23	0.07	2.27	0.14	0.34	0.60	0.38	0.82	1.35	0.45
Lu	0.07	0.02	0.32	0.08	0.09	0.12	0.04	0.01	0.34	0.02	0.05	0.09	0.05	0.13	0.19	0.07
Hf	0.03	0.06	0.16	0.09	0.36	0.38	0.78	0.19	0.36	0.07	0.07	0.27	0.28	0.48	0.45	0.07
Ta	1.21	0.45	0.39	0.15	0.15	0.22	0.32	0.78	0.43	0.16	0.19	1.77	0.48	0.48	0.37	0.38
W	399.07	431.98	590.3	392.4	348.9	372.6	200.3	442.3	502.94	148.95	294.02	278.33	309.53	430.8	239.4	525.3
Pb	81.70	61.54	8.21	6.57	8.26	12.41	25.68	35.96	7.32	13.41	13.96	26.04	19.01	8.11	12.09	6.10
Th	15.57	7.31	6.80	1.00	1.51	3.43	4.90	0.92	2.72	1.43	10.32	3.46	3.31	3.46	1.09	2.89
U	6.84	34.68	1.49	0.49	1.33	1.83	2.11	1.00	1.00	0.36	1.20	3.59	2.36	0.97	0.55	1.52
Th/Ta	12.9	16.2	17.3	6.74	10.3	15.7	15.2	1.18	6.28	9.10	54.2	1.95	6.88	7.15	2.90	7.61
Ba/Th	43.1	69.0	87.5	308.1	114.9	103.2	29.7	491.9	97.9	384.9	49.3	67.0	80.4	73.7	125.3	140.0
Ba/La	21.3	47.8	40.5	76.1	36.7	49.4	38.9	291.8	17.6	284.9	20.0	28.7	24.3	22.0	10.0	99.0
Th/Nb	2.41	2.04	2.11	0.23	0.51	0.71	1.32	0.35	0.38	0.68	4.47	0.17	0.45	0.82	0.17	0.41
Th/Yb	25.1	46.2	3.38	1.88	2.51	4.58	20.9	12.4	1.20	10.1	30.6	5.78	8.70	4.21	0.81	6.36
Nb/Yb	10.4	22.7	1.60	8.29	4.93	6.42	15.8	35.2	3.13	14.8	6.85	34.8	19.5	5.13	4.79	15.7
Yb+Ta	1.83	0.61	2.41	0.68	0.75	0.97	0.56	0.85	2.70	0.30	0.53	2.37	0.86	1.30	1.72	0.83